VOL. 16, NO. 22, NOVEMBER 2021 ISSN 1819-6608
ARPN Journal of Engineering and Applied Sciences

www.arpnjournals.com

TIME CONSTANT EFFECTS FOR FLUID-FUELED MOLTEN SALT REACTORS

G. Espinosa-Paredes[1], J. Domínguez-Alfaro[1], E.-G. Espinosa-Martínez[2] and A. Vázquez-Rodriguez[1]
[1]Área de Ingeniería en Recursos Energéticos, Universidad Autónoma Metropolitana-Iztapalapa, México City, México
[2]Departamento de Sistemas Energéticos, Facultad de Ingeniería, Universidad Nacional Autónoma de México, México
E-Mail: yurihillel@gmail.com

ABSTRACT

The aim of this work is to analyze the effects of the core and loop (external) time constants on the delayed-neutron precursors in fluid-fueled molten salt reactors (MSR). A 0-D mathematical model of neutron precursor concentration and neutron power without feedback effects is used for this analysis. For different time constants, we present the behavior of the precursors concentration, thermal power, and the external reactivity. According to the obtained results, we find that the external reactivity is small for large time constants in the core and in the external loop.

Keywords: molten salt reactor, point reactor kinetics, circulation fluid kinetics precursor; time delay, reactivity.

INTRODUCCION

The molten salt nuclear reactors (MSR) are high-efficiency reactors and one of the most promising concepts of the IV generation reactors. These are fission reactors that are in the fast or thermal spectrum and use a fluid mixture of molten salts as fuel and/ or coolant (Dolan, 2017). This type of reactors is often used with thorium or uranium fuel, which represents an advantage in technology, due to the large reserves of thorium existing in nature, it can also be used as a breeding reactor or for burning waste from existing reactors like PWRs and BWRs which would decrease the production of nuclear waste. In this technology, the fuel salt that can be uranium tetrafluoride (UF4) or thorium tetrafluoride (ThF4) is dissolved in a mixture of salts such as lithium fluoride with beryllium fluoride (LiF-BeF). The fuel salt enters the core with a temperature of around 650 C and recirculates in a time of approximately 5 seconds, while a fission chain reaction is carried out that reaches temperatures of up to 750 C and is moderated using graphite. The mixtures of salts used vary according to the design of the reactor (Muránsky *et al.*, 2019). There are designs of this technology in which the reactor core is coated with a salt of fertile material to produce fuel (Allibert *et al.*, 2016). In the MSR cycle, molten salts are generally used as fuel or as coolant. This technology is considered one of the safest, due that the salts (fuel/coolant) have high melting temperatures, if a molten salt leak occurs, it will freeze, and no radioactive materials will be released (Yoshioka *et al.*, 2017). Also, in this type of systems, there are underground storage tanks for the discharge of salts, in case the temperature in the core exceeds the established limits.

According to Wooten & Powers (2018), the interest in circulating fuel reactors, particularly molten salt reactors of the fluid fuel type, has been growing in the last two decades (e.g., Pázsit *et al*., 2014; Zhang et al., 2015; Betzler *et al.*, 2017), and more recently (e.g. Greenwood & Betzler, 2019; Dinamik 2019; Rykhlevskii *et al.*, 2019; Bajpai *et al*., 2020; Diniz et al., 2020; Greenwood et al., 2020).

The dynamics of the MSR have unique characteristics compared to conventional reactors (solid fuel made of multi-pellets contained in rods) because it is a circulating fuel reactor. The latter, due to the migration of delayed-neutron precursors in the circulating fuel, which is caused by delayed temperature feedback effects (Singh et al., 2020).

In this work we analyse delayed time effects (core and loop) in the dynamic behaviour of the molten salt reactor with a 0-D mathematical model without feedback effects.

MOLTEN SALT REACTOR DESCRIPTION

As opposed to conventional nuclear reactors that use solid fuels, in the molten salt reactors the salt mixture simultaneously acts as coolant and fuel. The molten salt circulates through the composite core, in this case graphite, where the flow at the outlet of the core has a higher temperature compared to the inlet. Then it circulates in an external circuit where the power generated by the fission is removed by heat exchangers. Because of geometric buckling, among other aspects, products do not generate fissions in the heat exchanger, however, concentration of the fission fragments and those of neutron precursors decay in the external circuit, which have an effect when they return to the nucleus of the reactor, an effect that is studied in detail in this work. In general, it is found that the movement of delayed neutron precursors through the primary loop has significant impact on transients at low reactor power or those with change in the primary loop mass flow rate (Wooten & Powers, 2018).

0-D MATHEMATICAL MODEL

Neutron density $n(t)$ for the 0-D mathematical model is given by point reactor kinetics equations:

$$\frac{dn}{dt} = \frac{\rho(t)-\beta}{\Lambda} n(t) + \lambda c(t) \quad (1)$$

which considers two contributions of neutrons, i.e., the first term on the hand right are the instantaneous neutrons

due to fission reactions and the second term is due to the decay of the fission fragments best known as neutron precursors. In this equation $\rho(t)$ is the reactivity that considers all the contributions like the external reactivity, and the physical effects of the molten salt fuel (temperature and density), β is the is the total fraction of delayed neutrons, Λ is the prompt neutron lifetime, and λ is the decay constant.

The concentration of delayed neutron precursors $c(t)$ model, in addition to consider to be fission fragments that emit neutrons and their disappearance due to the decay process, the model considers that these travel with the fluid inside the nucleus and outside it towards the heat exchangers or external loop (Sides, 1970).

$$\frac{dc}{dt} = \frac{\beta}{\Lambda} n(t) - \lambda c(t) - \frac{c(t)}{\tau_C} + \frac{c(t-\tau_L)}{\tau_C} e^{(-\lambda \tau_L)} \tag{2}$$

For purposes of rate change (with respect to time) analysis and physical meaning we will define each of these terms as follows:

$$\dot{C}_S = \frac{\beta}{\Lambda} n(t), \quad \textit{Fission source} \tag{3}$$

$$\dot{C}_D = -\lambda c(t), \quad \textit{Decay rate} \tag{4}$$

$$\dot{C}_O = -\frac{c(t)}{\tau_C}, \quad \textit{Outlet flow} \tag{5}$$

$$\dot{C}_I = \frac{c(t-\tau_L)}{\tau_C} e^{(-\lambda \tau_L)}, \quad \textit{Inlet flow} \tag{6}$$

where $\dot{C}_I$ and $\dot{C}_O$ are precursors atom flow rate inlet and outlet according by mass and momentum balances of the fluid in the reactor. Here, τ_C and τ_L are transient times through the core and the external loop, respectively (see Figure-1).

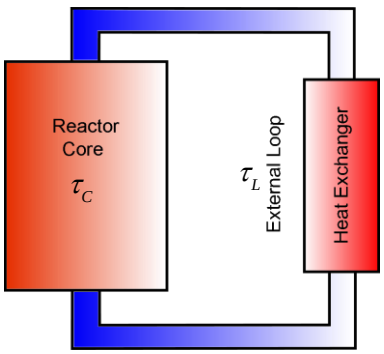

Figure-1. Schematic model of the reactor core with an external loop.

The initial conditions at $t = 0$ are given by:

$$n = n_0 \tag{7}$$

$$c_0 = \frac{\beta\, n_0}{\Lambda\left[\lambda + \frac{1}{\tau_c}\left(1 - e^{-\lambda \tau_L}\right)\right]} \tag{8}$$

The external reactivity due to control rods is obtained with the 0-D neutron density equation:

$$0 = \frac{\rho_0 - \beta}{\Lambda} n_0 + \lambda c_0 \tag{9}$$

Considering Eq. (8) into this equation:

$$\rho_0 = \beta - \frac{\beta}{1 + \frac{1}{\tau_c \lambda}\left(1 - e^{-\lambda \tau_L}\right)} \tag{10}$$

The reactor power is given by

$$P(t) = P_0\, n(t) \tag{11}$$

where P_0 is the reactor power at nominal conditions, and $n(t)$ is the normalized neutron density.

NUMERICAL SOLUTION

In order to obtain the numerical solution of the initial value problem the Euler method is applied:

$$\frac{dy}{dt} = f\left[y(t)\right], \quad y(t_0) = y_0 \tag{12}$$

where y, y_0 and f in general are vectors in n-dimensional real space, is sought by integrating from t_0 to $(t_0 + h)$, in the form:

$$y_{k+1} = y_k + \int_{t_0}^{t_0+h} f\left[y(x)\right] dx \tag{13}$$

i.e.

$$y_{k+1} = y_k + hf(t_k, y_k) \tag{14}$$

which is known as the forward Euler method. The stability of this method is obtained with the test equation:

$$\frac{dy}{dt} = \mu y \tag{15}$$

where μ is a complex number, and for non-trivial zero solution $y_0 \neq 0$. Then,

$$y_{k+1} = (1+h\mu)y_k \quad (16)$$

The exact solution of the test equation is given by:

$$y(t) = y_0 e^{\mu t} \quad (17)$$

when μ is such that its real part is negative [$\mathrm{Re}(\mu) < 0$], then the exact solution decay to 0 as t goes to infinite. Numerically it corresponds that y_k goes to 0 when k goes to infinite. In order to establish this stability criterion, it is necessary to satisfy the following inequality $|1+h\mu| < 1$, i.e., $-1 < 1+h\mu < 1$ or $-2 < h\mu < 0$ or $0 < h < -2/\mu$. Then, the stability condition for the forward Euler method is given by:

$$h < -\frac{2}{\mu} \quad (18)$$

METHODOLOGY

The main steps of the methodology are as follows:

Step 1. Input parameters: λ, β, τ_C and τ_L.

Step 2. Given the initial conditions of the neutron density n_0 we obtain the initial concentration c_0 given by (10).

Step 3. The external reactivity is calculated as:

$$\rho_{k+1} = \beta - \frac{\Lambda\lambda c_k}{n_k}, \; k = 0,1,2,\ldots n \quad (19)$$

when $k = 0$, Eq. (9) is obtained.

Step 4. The power, neutron density and precursor concentration are calculated:

$$n_{k+1} = n_k + hf(t_k, y_k) \quad (20)$$

$$c_{k+1} = c_k + hf(t_k, y_k) \quad (21)$$

$$P_{k+1} = P_0 n_{k+1} \quad (22)$$

Until $k = n$ or or until a new steady state is reached. Then, an experiment numerical is achieved.

Step 5. The following numerical experiment is carried out when the transient time through the core τ_C or the transient time through the external loop τ_L reach the stablished constants and the numerical simulation re-starts from **Step 2**.

RESULTS AND DISCUSSIONS

The numerical experiments were carried out with the following nuclear parameters: $\Lambda = 0.00036s$, $\beta = 0.0024$ and $\lambda = 0.0024s^{-1}$; the thermal power rate is $P_0 = 2.25GW$. The values of the core and loop time constants established in previous work are $\tau_C = 4s$ and $\tau_L = 6s$, respectively (Zarei, 2018).

Step Length

In order to establish the step length h of the Euler method, numerical experiments were performed considering $\tau_L = 6s$ with different values of τ_C and a simulation time of 20s. The results obtained are presented in Figure-2.

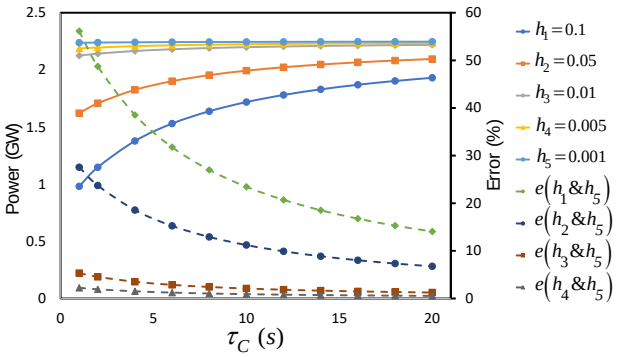

Figure-2. Thermal power and relative error for different values of step length h with $\tau_L = 6s$.

In this figure the thermal power $P(t)$ behaviour and the relative error associated are depicted for $h_1 = 0.1s$, $h_2 = 0.05s$, $h_3 = 0.01s$, $h_4 = 0.005s$ and $h_5 = 0.001s$, where the relative error is defined as:

$$Relative\ error = \lim_{t\to\infty} \left| \frac{P_{h_5}(t) - P_{h_x}(t)}{P_{h_5}(t)} \right| \times 100 \quad (23)$$

Here $P_{h_5}(t)$ is the thermal power obtained with h_5 and $P_{h_x}(t)$ with h_x where $x = 1,2,3,4$. In this equation $t \to \infty$, i.e., the relative error is obtained at steady state for each value of τ_C. In general, in this figure it can be observed that $P(t)$ for $h_1 = 0.1s$ presents a very large relative error for small τ_C values. The relative error decreases when τ_C increases. On the other hand, $P_{h_4}(t)$ and $P_{h_5}(t)$ are very close in behaviour with respect to $P_{h1}(t)$, $P_{h_2}(t)$ and $P_{h_3}(t)$ for all τ_C. According to the evidence of invariance of numerical results against the integration step, it is shown that $h_5 = 0.001s$ presents better accuracy. **Table 1** shows the comparison between $P_{h4}(t)$ and $P_{h5}(t)$, where the relative error is maximum

for $\tau_C = 1s$, and when $\tau_C = 20s$ the relative error is minimum.

Table-1. Comparison between h_4 and h_5.

τ_C (s)	P_{h_4} (GW)	P_{h5} (GW)	$error$ (%)
1	2.187	2.237	2.247
5	2.211	2.242	1.366
10	2.224	2.244	0.912
15	2.230	2.246	0.689
20	2.234	2.246	0.549

Numerical Experiments

Figures 3, 4 and 6 show the simulated behaviour of the thermal power, concentration of delayed precursors and external reactivity, respectively. As it can be observed in these figures, the behaviour is obtained as a function of τ_C for different values of τ_L.

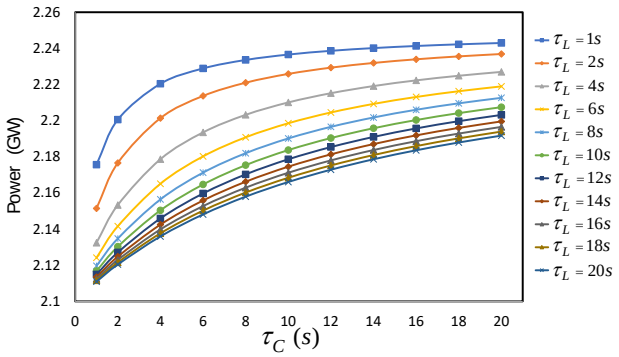

Figure-3. Thermal power vs τ_C for different values of τ_L.

According with the simulations the thermal power increases as the transient time in core τ_C increases for any constant value of τ_L, as the depicted in Figure-3. However, the differences between the estimated power and the design power of the MSR are important from a control theory point of view. The behaviour of the neutron precursors is directly proportional to the thermal power of the reactor, as depicted in Figure-4. The increase in precursors with increasing power is due to the fact that the production of fission fragments which predominate, rather than decay due to the emission of neutrons. It is important to highlight that the behaviour of the thermal power as shown in Figure-3, is caused by the balance between the input precursors (after passing through the external loop) and the output of the core.

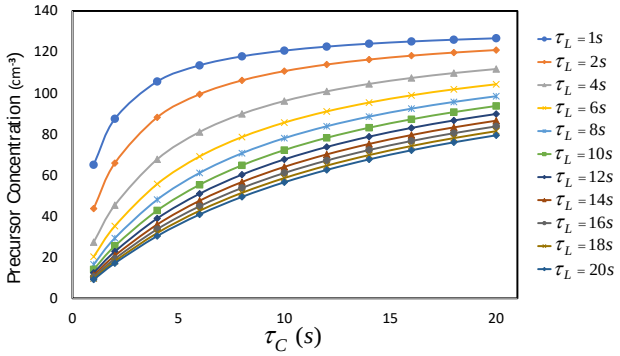

Figure-4. Precursor vs τ_C for different values of τ_L.

The behaviour of the external reactivity ρ_0 is inversely proportional to the thermal power of the reactor, as depicted in Figure-5. For large time constants both core reactor and external loop, the external reactivity presents very low reactivity values. Under these conditions, the ratio of total change of precursor concentration is minimal (Eq. 2), but it still has an influence on the reactor power.

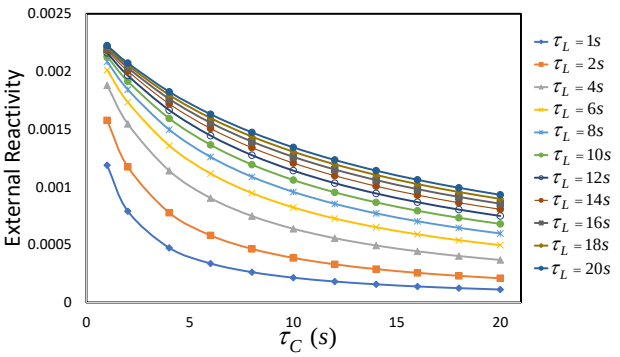

Figure-5. External reactivity vs τ_C for different values of τ_L.

Tables 2-4 present the external reactivity values for short, medium, and long times of the external loop, respectively. In these tables the values of external reactivity are lower for higher values of neutron concentration. For example, for $\tau_L = 1, 8, \text{ and } 16s$ (with $\tau_C = 16s$) the external reactivity is 0.000138, 0.000703 and 0.000981, respectively. It can also be observed in these tables that the difference in power between the nominal and that obtained in each numerical experiment is also smaller.

Table-2. External reactivity for $\tau_L = 1s$.

τ_C (s)	ρ_0	c_0	$P_0 - P(t)$ (GW)
1	0.001189	65.0314	0.0743
8	0.000262	117.878	0.0164
16	0.000138	125.134	0.0086

Table-3. External reactivity for $\tau_L = 8s$.

τ_C (s)	ρ_0	c_0	$P_0 - P(t)$ (GW)
1	0.002085	16.461	0.1303
8	0.001088	70.672	0.0680
16	0.000703	92.399	0.0439

Table-4. External reactivity for $\tau_L = 16s$.

τ_C (s)	ρ_0	c_0	$P_0 - P(t)$ (GW)
1	0.002201	10.362	0.1375
8	0.001393	53.757	0.0870
16	0.000981	76.640	0.0613

A more detailed analysis on the behaviour and contribution in the mechanisms of creation and disappearance of the neutron concentration is presented in Figure-6. This figure shows the change in concentration with respect to time, that is, the rate of change of the precursors of each of the of contributions such as generation, core inlet, decay, and core exit given by Eqs. (3)-(6).

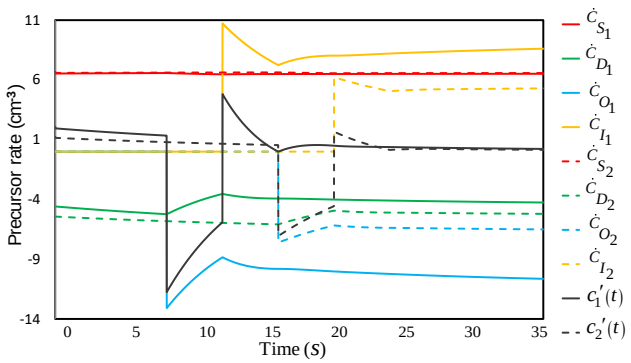

Figure-6. Precursor rate vs time elapsed for different values of $\tau_L = 4s$ and $\tau_{c_1} = 8s$; $\tau_{c_2} = 16s$

Two cases are presented in **Figure 6**, for medium and long transient times in the nucleus ($\tau_{c_1} = 8s$ and $\tau_{c_2} = 16s$) with $\tau_L = 4s$. In this figure c_1' and c_2' are given by Eq. (2) for each case analysed. In general, the rate of change of each contribution is greater for $\tau_{c_1} = 8s$ with respect to $\tau_{c_2} = 16s$. However, the fission term $\dot{C}_S$ is practically the same in both cases, due that the thermal power is about invariant. Then, the rate of change is summarized as follows: in general $|\dot{C}_O| > \dot{C}_I > \dot{C}_S > |\dot{C}_D|$ as expected $|\dot{C}_2|$ is greater than $|\dot{C}_{D1}|$ due to residence time τ_{c_2} is greater than τ_{c_1}.

CONCLUSIONS

In this work we analyze the effects of the fluid-fueled molten salt reactor delay time in the core and an external loop (heat exchanger) on the delayed-neutron precursor (Figure-4). The precursors concentration has an important effect in thermal power (Figure-3) and reactivity external (Figure-5). From the numerical results obtained we find that the external reactivity is small for large constant times in the core in combination with large constante time in the loops (e.g., Table-4). The rate chage of the outlet core precursor concentration is dominant respect to inlet core precursor concetration, source (due to fission) and precursor concentration decay. These analyzes are crucial in the design of control strategies in molten salt nuclear reactors.

ACKNOWLEDGEMENTS

The authors wish to thank the Research Seed of Computational Physics, the research group in Applied Physics FIASUR, and the academic and financial support of Universidad Surcolombiana.

REFERENCES

Allibert M., Aufiero M., Brovchenko M., Delpech S., Ghetta V., Heuer D., Laureau A. and Merle-Lucotte E. 2016. Molten Salt Fast Reactors. In I. L. Pioro. (Ed.), Handbook of Generation IV Nuclear Reactors (pp. 157-158). United Kingdom: Woodhead Publishing

Bajpai P., Lorenzi S. and Cammi A. 2020. A multiphysics model for analysis of inert gas bubbles in Molten Salt Fast Reactor. The European Physical Journal Plus. 135(6): 409.

Betzler B. R., Powers J. J. and Worrall A. 2017. Molten salt reactor neutronics and fuel cycle modeling and simulation with SCALE. Annals of Nuclear Energy. 101, 489-503.

Dinamik E. T. R. D. O. 2019. A new solution approach for the nonlinear dynamic model of molten salt reactors. Turkish Journal of Nuclear Science. 31(2).

Diniz R. C., da Cruz Gonçalves A. and da Rosa F. S. D. S. 2020. Neutron point kinetics model with precursors' shape function update for molten salt reactor. Nuclear Engineering and Design. 360, 110466.

Dolan T. 2017. Introduction. In T. Dolan (Ed.), Molten Salt Reactors and Thorium Energy. Woodhead Publishing: United Kingdom.

Greenwood M. S. and Betzler B. 2019. Modified Point-Kinetics Model for Neutron Precursors and Fission Product Behavior for Fluid-Fueled Molten Salt Reactors. Nuclear Science and Engineering. 193(4): 417-430.

Greenwood M. S., Betzler B. R., Qualls A. L., Yoo J. and Rabiti C. 2020. Demonstration of the Advanced Dynamic System Modeling Tool TRANSFORM in a Molten Salt

Reactor Application via a Model of the Molten Salt Demonstration Reactor. Nuclear Technology. 206(3): 478-504.

Muránsky O., Yang C., Zhu H., Karatchevtseva I., Sláma P., Nový Z. and Edwards L. 2019. Molten salt corrosion of Ni-Mo-Cr candidate structural materials for Molten Salt Reactor (MSR) systems. Corrosion Science, 108087.

Pázsit I., Dykin V. and Sanchez R. 2014. The point kinetic component of neutron noise in an MSR. Annals of Nuclear Energy. 64, 344-352.

Rykhlevskii, A., Bae, J. W., and Huff, K. D. (2019). Modeling and simulation of online reprocessing in the thorium-fueled molten salt breeder reactor. Annals of Nuclear Energy, 128, 366-379.

Sides Jr W. H. 1970. Control studies of a 1000-Mw (e) MSBR (No. ORNL-TM--2927). Oak Ridge National Lab.

Singh V., Wheeler A. M., Upadhyaya B. R., Chvála O. and Greenwood M. S. 2020. Plant-level dynamic modeling of a commercial-scale molten salt reactor system. Nuclear Engineering and Design. 360, 110457.

Wooten D. and Powers J. J. 2018. A review of molten salt reactor kinetics models. Nuclear Science and Engineering. 191(3): 203-230.

Yoshiok R., Kinoshita M. and Scott I. 2017. Materials. In: T. olan (Ed.) Molten Salt Reactors and Thorium Energy (pp. 189-193). Woodhead Publishing: United Kingdom.

Zarei M. 2018. Nonlinear dynamics and control in molten salt reactors. Nuclear Engineering and Design, 332, 289-296.

Zhang D., Rineiski A., Wang C., Guo, Z., Xiao Y. and Qiu, S. 2015. Development of a kinetic model for safety studies of liquid-fuel reactors. Progress in Nuclear Energy. 81, 104-112.